MATHEMATICAL APPROACH TO INVESTIGATE THE BEHAVIOUR OF THE PRINCIPAL PARAMETERS IN AXISYMMETRIC SUPERCAVITATING FLOWS, USING BOUNDARY ELEMENT METHOD

R. Shafaghat [*] **S. M. Hosseinalipour** [**] **N. M. Nouri** [***] **A. Vahedgermi** [****]

Department of Mechanical Engineering
Iran University of Science and Technology
Tehran, Iran

ABSTRACT

In this paper, a direct boundary element method (DBEM) is formulated numerically for the problems of the unbounded potential flows past supercavitating bodies of revolution (cones and also disks which are special case of cones with tip vertex angle of 180 degree) at zero degree angle of attack. In the analysis of potential flows past supercavitating cones and disks, a cavity closure model must be employed in order to make the mathematical formulation close and the solution unique. In the present study, we employ Riabouchinsky closure model. Since the location of the cavity surface is unknown at prior, an iterative scheme is used. Where, for the first stage, an arbitrary cavity surface is assumed. The flow field is then solved and by an iterative process, the location of the cavity surface is corrected. Upon convergence, the exact boundary conditions are satisfied on the body-cavity boundary. For this work, powerful software, based on CFD code, is developed in CAE center of IUST. The predictions of the software are compared with those generated by analytical solution and with the experimental data. The predictions of software for supercavitating cones and disks are seen to be excellent. Using the obtained data from software, we investigate the mathematical behavior of axisymmetric supercavitating flow parameters including drag coefficients of supercavitating cones and disks, cavitation number and maximum cavity width for a wide range of cone and disk diameters, cone tip angles and cavity lengths. The main objective of this study is to propose appropriate mathematical functions describing the behavior of these parameters. As a result, among all available functions such as linear, polynomial, logarithmic, power and exponential, only power functions can describe the behavior of mentioned parameters, very well.

Keywords : Supercavitation, Axisymmetric, Boundary element method.

1. INTRODUCTION

Supercavitation is a revolutionary means to achieve drag reduction up to 90% on an underwater body [1]. This level of drag reduction will have dramatic effects on the operation of naval forces. The high level of drag reduction is achieved by enveloping the body within a gaseous cavity. Only small area at the nose (cavitator) remains in contact with the liquid.

The study of axisymmetric supercavitating flow problems has always been of great interest, since they are in general more applicable to reality than 2-dimensional models. Of the early work on infinite-length axisymmetric supercavitating flow, we note Reichardt [2], who experimentally studied the axisymmetric supercavitating flows, and Garabedian [3], who developed an analytical method for calculating cavity shapes, though the accuracy of the method he presented is limited. Following the work on axisymmetric flow by Reichardt [2] and Garabedian [3], attention was paid to finite-length cavities springing from bodies of revolution by a number of authors, such as Cuthbert and Street [4], Brennen [5], Chou [6], Aitchison [7], Hase [8] and Varghese, Uhlman and Kirschner [9]. These authors used a variety of techniques for modeling the supercavitating flows including finite difference, finite element, boundary integral and interior source methods.

The most useful information from a solution of a supercavitating flow problem is the spatial location of the free surface (cavity surface) and knowledge of velocities and/or pressures along the boundaries. This realization leads one to feel that domain-type techniques (such as FDM and FEM) are computationally inefficient and that the problem is ideally suited to a boundary element method (BEM) solution [10].

The boundary element method is based on the descritization of an integral equation that, mathematically, is equal to the governing partial differential equation of the problem. The one of the main advantages of the boundary element method is that in which, instead of the whole domain, we generate the mesh only on the boundaries of the domain and so, the number of the

[*] Ph.D. student [**] Associate Professor, corresponding author [***] Assistant Professor [****] M.Sc. student

generated meshes reduces considerably. This advantage decreases the numerical solution run-time and solution costs [11].

At literatures such as [10,12] and [13] the authors deduced that for supercavitating flows, the BEM gives more accurate solutions than finite difference or finite element methods. Moreover, the method can, in most cases, provide an order of magnitude increase in efficiency over finite difference or finite element methods. As mentioned before, the gain in efficiency and ease of use is due to the fact that solution of the partial differential equation in the entire domain is reduced to the solution of an integral equation on the boundary of the domain.

In this study, we present a formulation of direct boundary element method for finding numerical solutions to axisymmetric supercavitating flows involving finite-length cavities. An example of such cavity is shown in Figs. 1 and 2, where we illustrate finite-length cavities with Riabouchinsky closure models behind a cone. It should be noted that this closure model has been chosen as a compromise between simplicity and physically validity [14]. According to the Riabouchinsky closure model, an image body is introduced at a certain distance downstream of the real body (cavitator) to make the cavity closed. Since the location of the cavity surface is unknown at prior, an iterative scheme is used. Where, for the first stage, an arbitrary cavity surface is assumed. The flow field is then solved and by an iterative process, the location of the cavity surface is corrected. Upon convergence, the exact boundary conditions are satisfied on the body-cavity boundary. The iterative scheme for determining the cavity surface position is similar to that of references [15,16]. It should be noted that, this problem is similar to a free-surface seepage flow problem. In reference [17], it was found that the number of iteration is fewer if one employs the hypersingular formulation than the singular formulation and FEM.

Because of the axial symmetry of the flow, only the quadrant of region needs to be considered in the numerical analysis [18]. By employing the Green's function, we substitute the boundary surface with a simple boundary line as shown in Fig. 3. The numerical solutions and iterative scheme mentioned above are performed by developed software based on CFD code. In this work, we investigate the mathematical behavior of axisymmetric supercavitating flow parameters including drag coefficient of supercavitating cones and disks, cavitation number and maximum cavity width for a wide range of cone and disk diameters, cone tip angles and cavity lengths. The main objective is to propose appropriate mathematical functions describing the behaviour of mentioned parameters.

2. MATHEMATICAL FORMULATION

Consider the unbounded, steady and irrotational flow of an inviscid and incompressible liquid past a supercavitating cone placed at zero degree angle of attack in the flow direction (Fig. 1). The flow is then a potential flow and hence possesses a potential function, Φ, which in the fluid satisfies Laplace's equation:

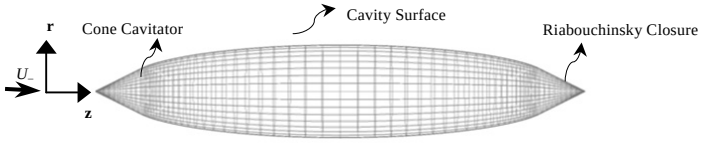

Fig. 1 Side view of finite-length cavity with Riabouchinsky closure model

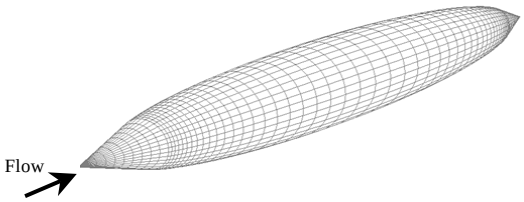

Fig. 2 Isometric view of finite-length cavity with Riabouchinsky closure model

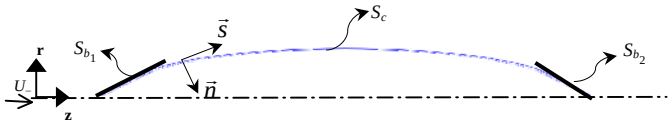

Fig. 3 The boundary of solution

$$\nabla^2\Phi = \frac{\partial^2\Phi}{\partial r^2} + \frac{1}{r}\frac{\partial\Phi}{\partial r} + \frac{\partial^2\Phi}{\partial z^2} = 0 \tag{1}$$

Where Φ is the total potential. A disturbance potential, φ, can be defined from the total potential by:

$$\Phi = U_\infty z + \varphi \tag{2}$$

Where U_∞ is the free stream velocity. So that the disturbance velocity is given by the gradient of the disturbance potential, the disturbance potential also obeys the Laplace's equation:

$$\nabla^2\varphi = \frac{\partial^2\varphi}{\partial r^2} + \frac{1}{r}\frac{\partial\varphi}{\partial r} + \frac{\partial^2\varphi}{\partial z^2} = 0 \tag{3}$$

3. BOUNDARY CONDITIONS

The requirement that the flow be tangential to the cavity and body surface (S_c and $S_b = S_{b_1} + S_{b_2}$) gives the following kinematic condition on the body-cavity surface, $\Gamma = S_c + S_b$:

$$\frac{\partial\Phi}{\partial\vec{n}} = 0 \quad \text{on} \quad \Gamma\,. \tag{4}$$

Where $\vec{n} = n_z\,\hat{e}_z + n_r\,\hat{e}_r$ is the unit vector normal to the body-cavity surface (Fig. 3). Combining Eq. (2) with (4) gives:

$$\frac{\partial\varphi}{\partial\vec{n}} = -\vec{n}\cdot\vec{U}_\infty \quad \text{on} \quad \Gamma\,. \tag{5}$$

Similarly, a dynamic boundary condition (constant pressure) must be applied on the cavity surface, S_c. Using Bernoulli's equation, it may be shown that this condition becomes:

$$\frac{\partial \Phi}{\partial \vec{s}} = U_\infty \sqrt{1+\sigma} \quad \text{on} \quad S_c \tag{6}$$

Where, $\vec{s} = s_z\,\hat{e}_z + s_r\,\hat{e}_r$ is the unit vector tangent to the body-cavity surface (Fig. 3) and σ is the cavitation number. Combining Eq. (2) with (6) gives:

$$\frac{\partial \varphi}{\partial \vec{s}} = U_\infty \sqrt{1+\sigma} - U_\infty\, S_z \quad \text{on} \quad S_c \tag{7}$$

4. DIRECT BOUNDARY ELEMENT FORMULATION

In the DBEM formulation, a boundary integral equation is derived from Laplace's Eq. (3) through application of Green's second theorem. In axisymmetric flow, it has the following form:

$$\frac{1}{4\pi}\,\varphi(\vec{R}_0) + \int_\Gamma \varphi(\vec{R}) \frac{\partial G(\vec{R},\,\vec{R}_0)}{\partial \vec{n}}\, r_Q\, d\Gamma(\vec{R}) = -\int_\Gamma G(\vec{R},\,\vec{R}_0)\, n_z\, r_Q\, d\Gamma(\vec{R}) \qquad (\vec{R},\,\vec{R}_0) \in \Gamma \tag{8}$$

Where $\vec{n}$ is the unit vector normal to the body-cavity surface, $\vec{R}_0$ is the position vector of an interior 'load' point or 'source' point with coordinates (r_p, θ_p, z_p), $\vec{R}$ is the position vector of a 'field' point with coordinates (r_Q, θ_Q, z_Q) and $\partial G(\vec{R},\,\vec{R}_0)/\partial \vec{n}$ and $G(\vec{R},\,\vec{R}_0)$ are the first and second kernels respectively and defined as follows:

$$\frac{\partial G(\vec{R},\,\vec{R}_0)}{\partial \vec{n}} = \frac{1}{4\pi^2 r_Q C}\, n_r\, K\left(m,\,\frac{\pi}{2}\right) - \frac{r_p^2 - r_Q^2 + (z_p - z_Q)^2}{4\pi^2 r_Q C D}\, n_r\, E\left(m,\,\frac{\pi}{2}\right) - \frac{(z_p - z_Q)}{2\pi^2 C D}\, n_z\, E\left(m,\,\frac{\pi}{2}\right) \tag{9}$$

$$G(\vec{R},\,\vec{R}_0) = \frac{1}{2\pi^2 C} K\left(m,\,\frac{\pi}{2}\right) \tag{10}$$

Here $K(m, \pi/2)$ is the complete elliptic integral of the first kind, $E(m, \pi/2)$ is the complete elliptic integral of the second kind and parameters C, m and D are defined as follows:

$$C = \sqrt{(r_p + r_Q)^2 + (z_p - z_Q)^2} \tag{11}$$

$$m = \frac{2\sqrt{r_p\, r_Q}}{C} \tag{12}$$

$$D = (r_p - r_Q)^2 + (z_p - z_Q)^2 \tag{13}$$

5. NUMERICAL SOLUTION

For the numerical solution of the problem, we guess an initial cavity boundary location (Fig. 4). Then the body-cavity boundary, Γ, (ABCD in Fig. 4) is subdivided into a number of straight elements. The mesh concentration is higher near the points *B* and *C* (Fig. 4) because of singularity in these points. Linear interpolation functions are then introduced to relate the variation of the functions within each element to their values at the nodal points.

The symmetry axis (AD in Fig. 4) was taken into account by reflection and condensation as discussed by Brebbia *et al.* [18]. This is similar to considering image sources and avoids the discretization of the symmetry axis. Thus, the discretized version of Eq. (8) becomes:

$$\sum_{j=1}^{N}\left[\frac{1}{4\pi}\varphi_j\,\delta_{ij} + \varphi_j \int_{\Gamma j} \frac{\partial G_{ij}}{\partial \vec{n}_j}(\vec{R}_j \cdot \hat{e}_r)\, d\Gamma_j\right] = -\sum_{j=1}^{N}\int_{\Gamma j} (\vec{R}_j \cdot \hat{e}_r)(\hat{e}_z \cdot \vec{n}_j)\, G_{ij}\, d\Gamma_j \tag{14}$$

$$\delta_{ij} = \begin{cases} 1 & if \quad i = j \\ 0 & if \quad i \neq j \end{cases} \tag{15}$$

The symbol G_{ij} means the Green's function with the source point at the centroid of the i^{th} element and with the field point varying over all locations in the j^{th} element as the integration is carried out. In the above discretized equation, the only unknowns are the values of φ on the *N* element centroids. So, there will be *N* equations. Define:

$$A_{ij} = \frac{\delta_{ij}}{4\pi} + \int_{\Gamma j} \frac{\partial G_{ij}}{\partial \vec{n}_j}(\vec{R}_j \cdot \hat{e}_r)\, d\Gamma_j \tag{16}$$

and

$$B_i = -\sum_{j=1}^{N}\int_{\Gamma j} (\vec{R}_j \cdot \hat{e}_r)(\hat{e}_z \cdot \vec{n}_j)\, G_{ij}\, d\Gamma_j \tag{17}$$

Then, the final set of equations for the *N* values of φ is:

$$\sum_{j=1}^{N} A_{ij}\,\varphi_j = B_i \tag{18}$$

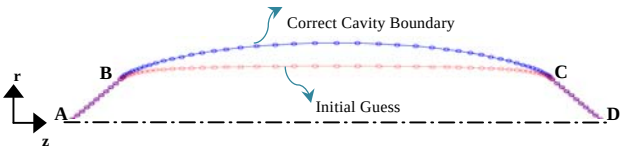

Fig. 4 Discretized body-cavity boundary

The DBEM solution then produces the values of disturbance potential at each node along the body-cavity boundary (ABCD in Fig. 4). The central problem is calculation of the velocity at the body-cavity boundary. At each node, *j*, the total flow is tangent to the body-cavity boundary so we need only find tangential velocity. The tangential velocity is the tangential derivative of the total potential, Φ (perturbation potential plus any exterior potential such as $U_\infty x$ for the steady flow problems we have been considering). For axisymmetric flows the tangential velocity component has a single direction at each node. We know how to determine the tangential derivative at a point using a modified central difference procedure for smooth objects. Even when the object has a sharp edge or tip (*A*, *B*, *C* and *D* in Fig. 4), this procedure can be used for all nodes except for those adjacent to a sharp edge. In addition, the numerical derivative can be determined at a point that is midway between the first and second nodes from the sharp edge. Then the tangential derivative can be approximated at a node nearest the sharp edge by numerical extrapolation. The obtained values for velocity at nodes on the cavity boundary are all equal for the correct cavity boundary position shown in Fig. 4 (but, of course, not for the assumed one), and it is essential that a procedure be devised to properly move the cavity boundary in the steps of the iteration scheme so that the constant-velocity or constant pressure condition be more closely satisfied on the moved boundary (Fig. 5). The iterative scheme here is the one employed by Shafaghat *et al.* [14,16].

As mentioned above, with respect to an initial guess and using an iteration scheme, we can reach to correct cavity boundary. To investigate how does the initial guess affect the solution and convergence, we consider the axisymmetric supercavitating flow around a cone (with tip angle of 100 degree, dimensionless base diameter of 1 and dimensionless cavity length of 10) and guess two initial cavity boundary locations including a straight line (Fig. 6) and a curve (Fig. 7). However, as shown in the below (Figs. 6 and 7), the solution are independent of initial guesses and both cases converge to the same solution. But, as shown in Figs. 8 and 9, when the initial guess is a curve, the solution converges more quickly (low iteration number).

It should be noted that the convergence of the iteration is dependent on the initial guessed curve for the location of the cavity surface. In fact, if the initial guess is poor, the iteration may not converge at all. Therefore, it is beneficial to have a method for generating the initial guess for the cavity surface, capable of reducing the computational costs. In this work, the initial guess for the cavity surface is generated by considering the points of cavity surface detachment (point *B* in the Fig. 4) and cavity surface reattachment (point *C* in the Fig. 4) and then fitting an arc of a circle through these points, which is tangent to the body at these points (Points *B* and *C* in Fig. 4).

6. ITERATION PROCEDURE

According to the previous subsection, the iteration procedure will be as follows:

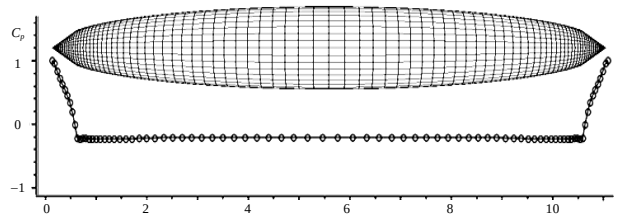

Fig. 5 Pressure coefficient distribution on the body-cavity surface

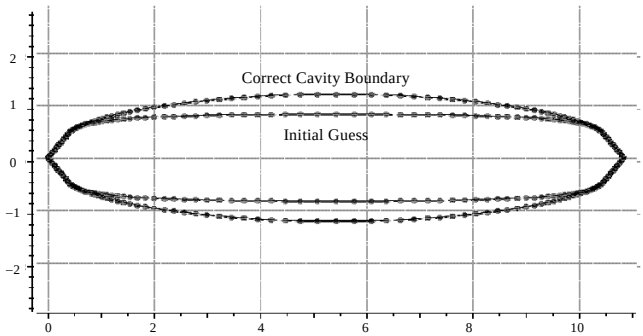

Fig. 6 Converged cavity boundary for curve as initial guess

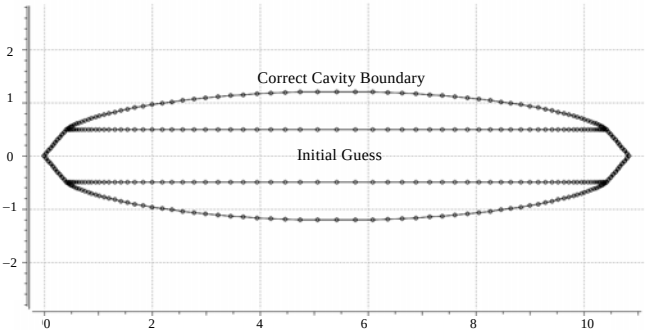

Fig. 7 Converged cavity boundary for straight line as initial guess

1. Assume an initial cavity boundary location.
2. DBEM solution provides value of velocity at each cavity boundary node (q_{c_i}).
3. Calculate the displacement of each node (in direction of *r* coordinate in Fig. 4), using the following empirical relation:

$$\Delta r_i = \omega \frac{|500 q_B^2 - 500 q_{Ci}^2|}{1000} r_i^3 \qquad (19)$$

Where ω is a relaxation parameter, q_{c_i} is the value of velocity at *i*th node on the cavity boundary and q_B is the value of velocity at point *B* (Fig. 4), the separation point. This value was selected because point *B* is a fixed cavity boundary point.

4. Compute the relative norm of increments
5. $Norm = \sum_{i=1}^{N} \frac{1}{N} \left| \frac{r_i^{k+1} - r_i^k}{r_i^k} \right|$

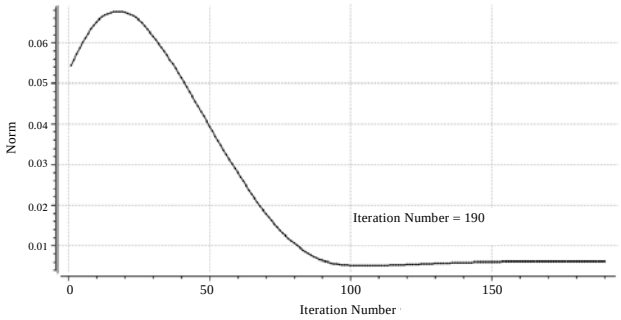

Fig. 8 Norm per iteration diagram for curve as initial guess

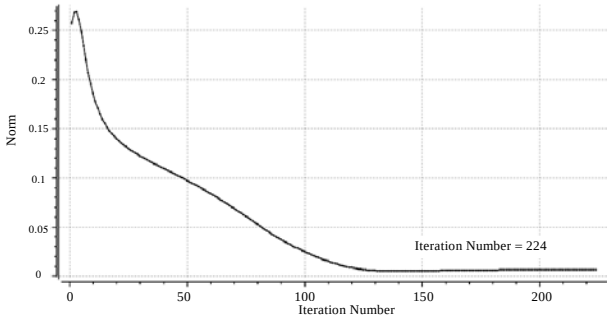

Fig. 9 Norm per iteration diagram for straight line as initial guess

Where N is the number of cavity boundary nodes. If the norm is smaller than a specified tolerance ε, the process has converged and is terminated; otherwise, the cavity boundary is moved to a new location given by $r_i^{k+1} = r_i^k + \omega \Delta r_i^{k+1}$ and the process returns to step (2).

7. RESULTS DISCUSSION

Numerical (DBEM) results are compared with analytical and experimental data, showing the superior accuracy of the direct boundary element method. The experimental data are taken from water-tunnel by Self and Ripken [19] (for cones with half- angles of 22.5 and 35 degree and base diameters of 1-in) and the analytical data are obtained by Hase [8] (for a cone with half angle of 45 degree and base diameter of 1.414-in). In Figs. 10 to 15, we compare the numerical results of the axisymmetric supercavitating flows past the cones with analytical and experimental data, showing a little discrepancy between them. Using the trial and error method, we deduced that the best value of the relaxation parameter (ω), to control the oscillations, is ω = 0.05.

After examining the accuracy of numerical method (DBEM), we investigate the mathematical treatment of important parameters of axisymmetric supercavitating flows including drag coefficient of supercavitating cones and disks, cavitation number and maximum cavity width for a wide range of cone and disk diameters, cone tip angles and cavity lengths. To do this, we fit various functions (such as Linear, logarithmic, polynomial, power and exponential) to data obtained from DBEM. As a result, in all cases the best and physically meaningful mathematical functions to show the treatment of parameters of supercavitating flows, around the cones and disks, are the power functions. The variables, in these functions, are cone half-angle (β) and dimensionless length of cavity (l_{cav}/D_b). These functions are as follows:

$$\sigma\left(\beta,\ \frac{l_{cav}}{D_b}\right) = f_1(\beta)\left(\frac{l_{cav}}{D_b}\right)^{f_2(\beta)} \tag{19}$$

$$\frac{D_{cav}}{D_b}\left(\beta,\ \frac{l_{cav}}{D_b}\right) = g_1(\beta)\left(\frac{l_{cav}}{D_b}\right)^{g_2(\beta)} \tag{20}$$

$$C_D\left(\beta,\ \frac{l_{cav}}{D_b}\right) = h_1(\beta)\left(\frac{l_{cav}}{D_b}\right)^{h_2(\beta)} + h_3(\beta) \tag{21}$$

Where the functions $f_1(\beta)$, $f_2(\beta)$, $g_1(\beta)$, $g_2(\beta)$, $h_1(\beta)$, $h_2(\beta)$ and $h_3(\beta)$ are defined as follows:

$$f_1(\beta) = 0.2087\ \beta^{0.3687} \tag{22}$$

$$f_2(\beta) = -10^{-5}\ \beta^2 + 0.0016\ \beta - 0.8979 \tag{23}$$

$$g_1(\beta) = 0.382\ \beta^{0.2612} \tag{24}$$

$$g_2(\beta) = 7\times10^{-6}\ \beta^2 - 0.0012\ \beta + 0.3941 \tag{25}$$

$$h_1(\beta) = -10^{-5}\ \beta^3 + 0.0018\ \beta^2 - 0.0902\ \beta + 2 \tag{26}$$

$$h_2(\beta) = -8\times10^{-7}\ \beta^4 + 0.0002\ \beta^3 - 0.0179\ \beta^2 + 0.6728\ \beta - 10 \tag{27}$$

$$h_3(\beta) = -7\times10^{-5}\ \beta^2 + 0.0169\ \beta - 0.096 \tag{28}$$

The functions (22) to (28) are obtained by the authors. The method of developing the functions $f_1(\beta)$ and $f_2(\beta)$ is explained here as typical instants. For different values of β, the function (19) generally has the following form:

$$\sigma\left(\beta_i,\ \frac{l_{cav}}{D_b}\right) = f_1(\beta_i)\left(\frac{l_{cav}}{D_b}\right)^{f_2(\beta_i)} = \sigma\left(\frac{l_{cav}}{D_b}\right)$$

Where $f_1(\beta_i)$ and $f_2(\beta_i)$ are the constant values. To derive f_1 and f_2 as a function of β, the points of $(\beta_i, f_1(\beta_i))$ and $(\beta_i, f_2(\beta_i))$ are mapped on the planes $(\beta - f_1)$ and $(\beta - f_2)$ respectively. To formulate the pattern of functions $f_1(\beta)$ and $f_2(\beta)$, different functions such as linear, polynomial, logarithmic, power and exponential are fitted on the points of $(\beta_i, f_1(\beta_i))$ and $(\beta_i, f_2(\beta_i))$. Subsequently, it is found that the power and polynomial functions are the most appropriate estimations for $f_1(\beta)$ and $f_2(\beta)$ respectively. The procedure is the same for the functions (24) to (28).

To verify the accuracy of obtained functions, we compare their results with the numerical (DBEM), analytical and experimental results as shown below (Figs. 16 to 24):

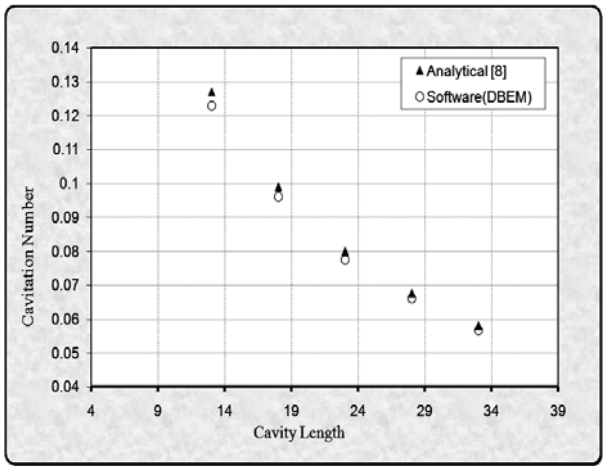

Fig. 10 Cavitation numbers for cavities of various lengths behind cone with half-angle 45° and base diameter of 1.414-in

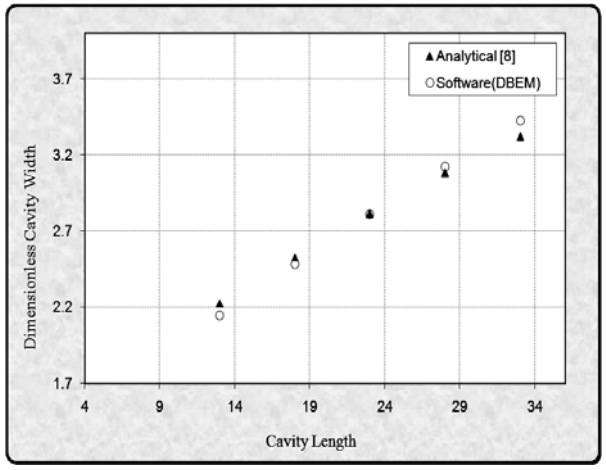

Fig. 11 Dimensionless cavity widths for cavities of various lengths behind cone with half-angle 45° and base diameter of 1.414-in

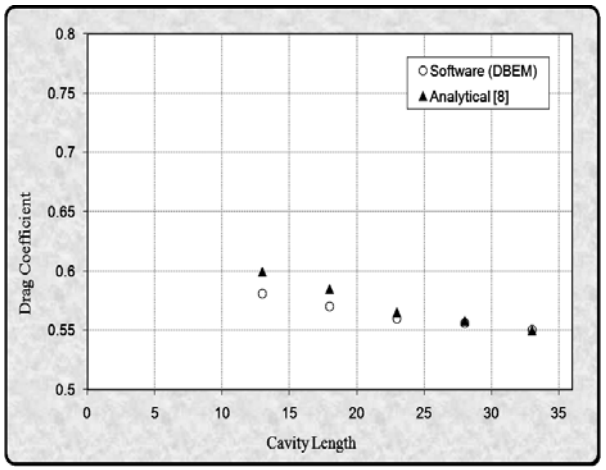

Fig. 12 Coefficient of drag for cavities of various lengths behind cone with half-angle 45° and base diameter of 1.414-in

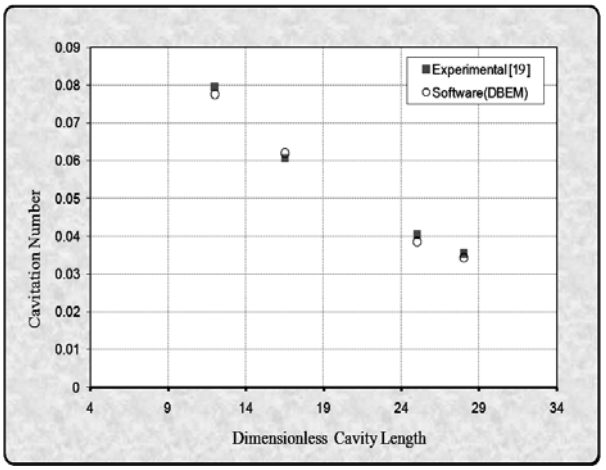

Fig. 13 Cavitation numbers for cavities of various lengths behind cone with half-angle 22.5° and base diameter of 1-in

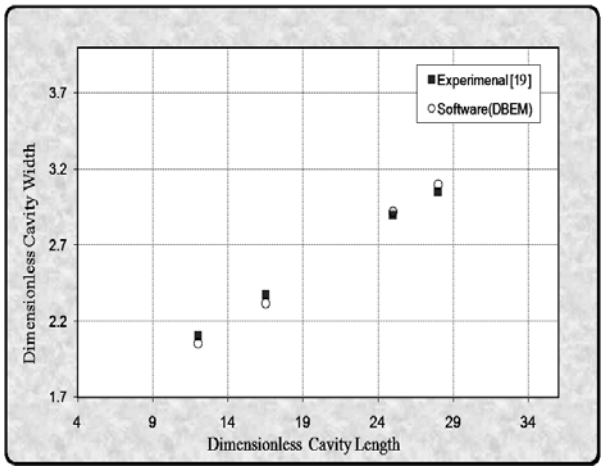

Fig. 14 Dimensionless cavity widths for cavities of various lengths behind cone with half-angle 22.5° and base diameter of 1-in

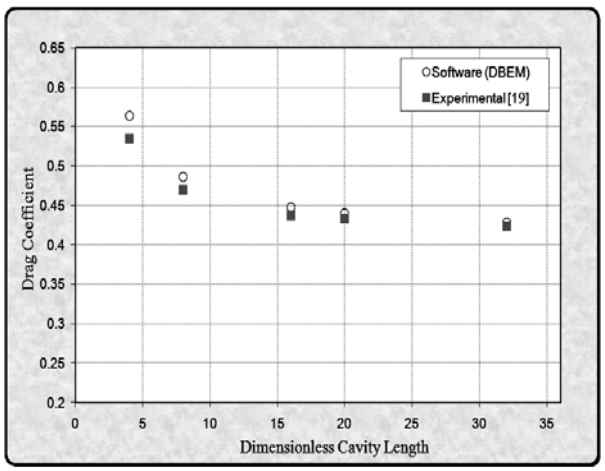

Fig. 15 Coefficient of drag for cavities of various lengths behind cone with half-angle 35° and base diameter of 1-in

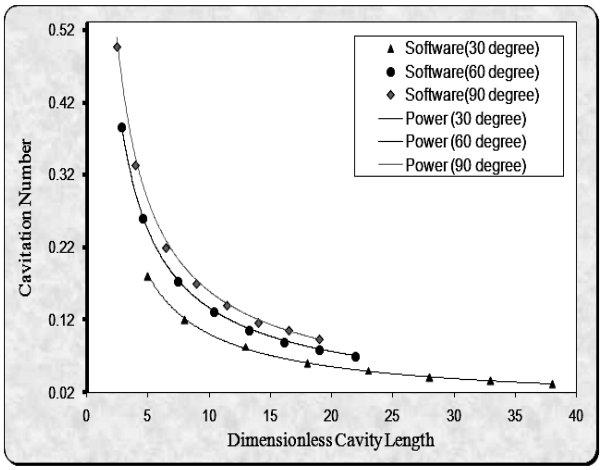

Fig. 16 Cavitation numbers for cavities of various lengths behind cones with half-angles 30°, 60° and 90°

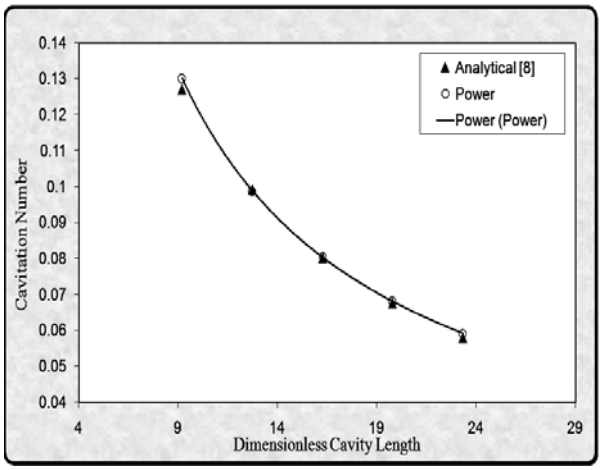

Fig. 19 Cavitation numbers for cavities of various lengths behind cone with half-angle 45° and base diameter of 1.414-in

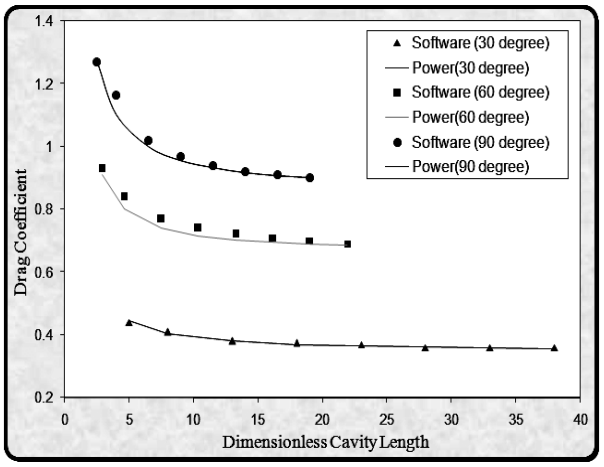

Fig. 17 Coefficient of drag for cavities of various lengths behind cones with half-angles 30°, 60° and 90°

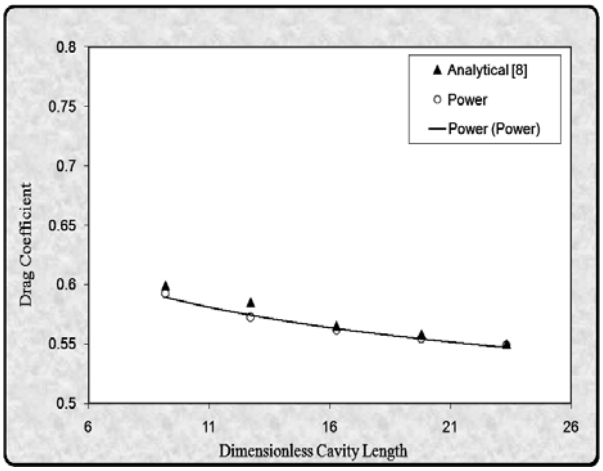

Fig. 20 Coefficient of drag for cavities of various lengths behind cone with half-angle 45° and base diameter of 1.414-in

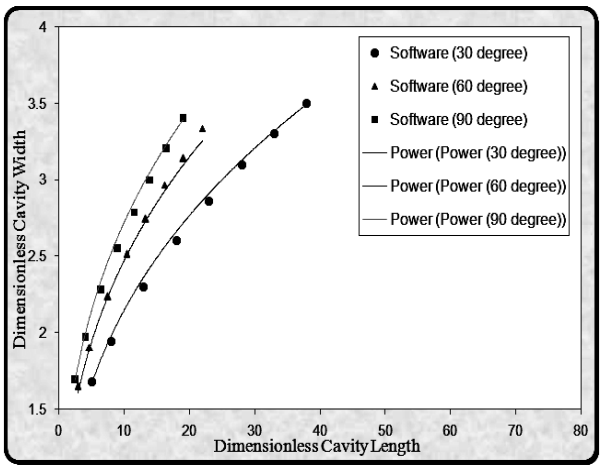

Fig. 18 Dimensionless cavity widths for cavities of various lengths behind cones with half-angles 30°, 60° and 90°

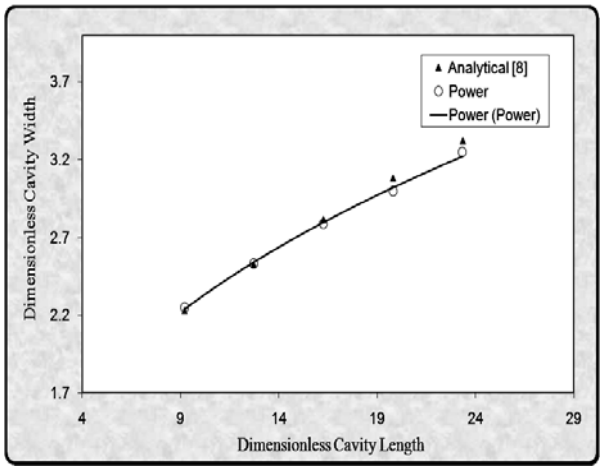

Fig. 21 Dimensionless cavity widths for cavities of various lengths behind cone with half-angle 45° and base diameter of 1.414-in

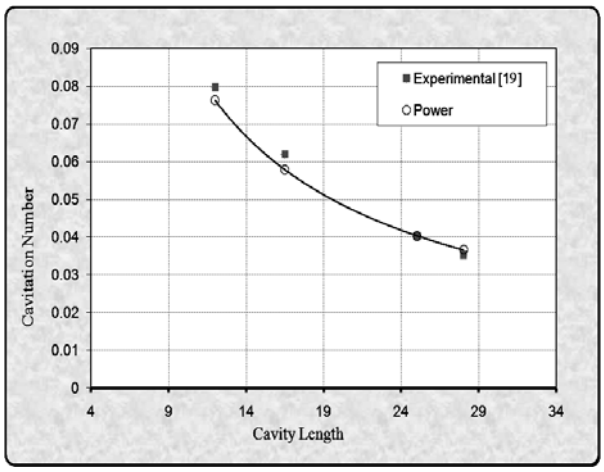

Fig. 22 Cavitation numbers for cavities of various lengths behind cone with half-angle 22.5° and base diameter of 1-in

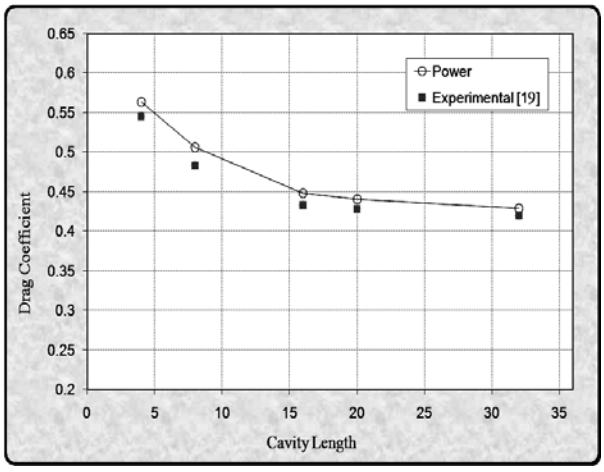

Fig. 23 Coefficient of drag for cavities of various lengths behind cone with half-angle 35° and base diameter of 1-in

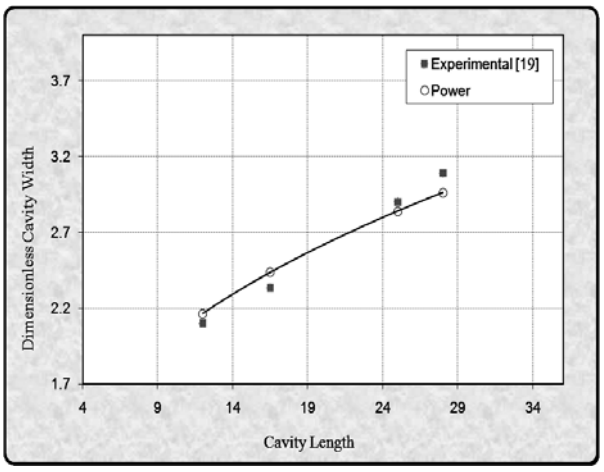

Fig. 24 Dimensionless cavity widths for cavities of various lengths behind cone with half-angle 22.5° and base diameter of 1-in

8. CONCLUSIONS

Considering above comparisons, we conclude that the obtained functions are capable of describing the behavior of axisymmetric supercavitating flow parameters (including drag coefficient, cavitation number and maximum cavity width) for various cones and disks accurately. Also, among all available functions such as linear, polynomial, logarithmic, power and exponential, only power functions can fit to obtained data very well. As the developed software has the ability of solving axisymmetric supercavitating flow around cavitators with various geometries, by employing the same process, we hope to obtain the mathematical behavior of axisymmetric supercavitating flow parameters for all types of axisymmetric cavitators additionally.

REFERENCES

1. Kuklinski, R., Henoch, C. and Castano, J., "Experimental Study of Ventilated Cavities on Dynamic Test Model," Naval Undersea Warfare Center, Cav2001: Session B3.004 (2001).
2. Reichardt, H., "The Physical Laws Governing the Cavitation Bubbles Produced Behind Solids of Revolution in a Fluid Flow," The Kaiser Wilhelm Institute for Hydrodynamic Research, Gottingen, Rep. UM 6628 (1945).
3. Garabedian, P. R., "The Calculation of Axially Symmetric Cavities and Jets," *Pacific Journal of Mathematics*, 6, pp. 611−689 (1956).
4. Cuthbert, J. and Street, R., "An Approximate Theory for Supercavitating Flow About Slender Bodies of Revolution," LMSC Report TM81-73/39, Lockheed Missiles and Space Co., Sunnyvale, California (1964).
5. Brennen, C. A., "Numerical Solution of Axisymmetric Cavity Flows," *Journal of Fluid Mechanics*, 37, pp. 4, 671−688 (1969).
6. Chou, Y. S., "Axisymmetric Cavity Flows Past Slender Bodies of Revolution," *Journal of Hydronautics*, 8, pp. 13−18 (1974).
7. Aitchison, J. M., "The Numerical Solution of Planar and Axisymmetric Cavitational Flow Problems," *Computers and Fluids*, 12, pp. 55−65 (1984).
8. Hase, P. M., Interior Source Methods for Planar and Axisymmetric Supercavitating Flows, Thesis submitted for the Degree of Doctor of Philosophy (2003).
9. Verghese, A. N., Uhlman, J. S. and Kirschner, I. N., "Numerical Analysis of High – Speed Bodies in Partially Cavitation Axisymmetric Flow," *Transactions of ASME, Journal of Engineering*, 127, pp. 41−54 (2005).
10. Wrobel, L. C., "A Simple and Efficient BEM Algorithm for Planar Cavity Flows," *International Journal for Numerical Methods in Fluids*, 14, pp. 524−537 (1992).
11. Becker, A. A., "The Boundary Element Method in Engineering," McGraw- Hill Book Company (1992).
12. Kennon, S. R., "Boundary Element Method," *Graduate*

Research Assistant, Dept. of Aerospace Engineering and Engineering Mechanics, University of Texas at Austin, Austin, TX. (1986).

13. Mukherjee, S. and Morjaria, M., "On the Efficiency and Accuracy of the Boundary Element Method," *International Journal For Numerical Methods In Engineering*, 20, pp. 515–522 (1984).
14. Kirschner, I. N., Fine, N. E., Uhlman, J. S., and Kring, D. C., Numerical Modeling of Supercavitating Flows, Paper presented at the RTO AVT lecture series on "Supercavitating Flows", held on the Von Karman Institute (VKI) in Belgium, and published in RTO EN-010, pp. 12–16 (2001).
15. Shafaghat, R., Hosseinalipour, S. M. and Shariatifard, A., "Numerical Analysis of a Two Dimensional Bounded Supercavitation Flow," 15th Annual Conferences of the CFD Society of Canada, Toronto, Canada pp. 27–31 (2007).
16. Shafaghat, R., Hosseinalipour, S. M. and Shariatifard, A., "Numerical Analysis of Two-Dimensional Supercavitation Flow Using a Boundary Element Method," *Journal of Numerical Simulations in Engineering*, University of Mazandaran, pp. 216–223 (2008).
17. Chen, J. T., Hsiao, C. C. and Chen, K. H., "Study of Free Surface Seepage Problems Using Hypersingular Equations," *Communications in Numerical Methods in Engineering*, 23, pp. 755–769 (2007).
18. Brebbia, C. A., Telles, J. C. F and Wrobel, L. C., Boundary Element Techniques. Springer, Berlin (1984).
19. Self, M. and Ripken, J. F., Steady-State Cavity Studies in a Free-jet Water Tunnel, St. Anthony Falls Hydr. Lab. Rep. 47 (1955).

(Manuscript received July 7, 2008,
accepted for publication February 15, 2009.)